Chinese Journal of Chemical Engineering 55 (2023) 34–40

Contents lists available at ScienceDirect

Chinese Journal of Chemical Engineering

journal homepage: www.elsevier.com/locate/CJChE

Full Length Article

Self-deposition for mesoporous carbon nanosheet with supercapacitor application

Juan Du [1], Aibing Chen [1,*], Senlin Hou [2,*], Xueqing Gao [1]

[1] College of Chemical and Pharmaceutical Engineering, Hebei University of Science and Technology, Shijiazhuang 050018, China
[2] The Second Hospital of Hebei Medical University, Shijiazhuang 050000, China

ARTICLE INFO

Article history:
Received 30 October 2021
Received in revised form 27 April 2022
Accepted 28 April 2022
Available online 6 May 2022

Keywords:
Monomer self-deposition
$Mg(OH)_2$ catalysis
Hard template
Carbon nanosheet
Supercapacitor

ABSTRACT

Porous carbon sheets have wide application prospects in many fields, especially in energy storage of supercapacitor due to the features combining both 2D structure and porous architectures. Herein, a self-deposition approach is proposed to obtain N-doped mesoporous carbon nanosheets (N-MCNs), using 3-aminophenol (3-AF) as precursor and $Mg(OH)_2$ sheet as hard template. This process realizes the direct carbon formation using 3-AF monomer as carbon precursor under the catalysis of hard template avoiding the polymerization and utilization of solvent. The mass ratio of 3-AF to $Mg(OH)_2$ plays an important role in determining the pore structures and the resulting capacitance behavior. The results show that N-MCNs with a mass ratio of 3-AF and $Mg(OH)_2$ of 1:1 have good electrochemical behavior for supercapacitors. This N-MCNs based electrode exhibits a high capacitance of 240 $F{\cdot}g^{-1}$ at 1 $A{\cdot}g^{-1}$, good rate performance (75.4% retention ratio at 20 $A{\cdot}g^{-1}$), and high cycling stability with 98.3% initial capacitance retained after 10000 cycles. Symmetric supercapacitors on N-MCNs achieve energy density of 18.2 $W{\cdot}h{\cdot}kg^{-1}$ and power density of 0.4 $kW{\cdot}kg^{-1}$ operated within a wide potential range of 0–1.6 V in 1.0 $mol{\cdot}L^{-1}$ Na_2SO_4 solution, exhibiting its potential for electrode materials with high performance.

1. Introduction

Porous carbon materials have attracted extensive attention in science and technology in recent years because of their high surface areas, excellent electrical conductivity, chemical stability and grading performance [1,2]. Especially, owing to their excellent electrical conductivity, tailor ability, inexpensiveness and versatility, porous carbon materials have been obtained widely attention in supercapacitor [3,4]. Based on the differences in the structures and surface properties of porous carbon materials and the electron/ion transport mechanism, porous carbon materials with different sizes and structures would exhibit different electrochemical properties [5–8]. Moreover, among the functionalized carbon materials, the nitrogen-doped ones with electrochemically active nitrogen species are intensively investigated. N-containing functional groups can increase the electronic charge density of graphene and favor proton adsorption in the acidic electrolyte.

Among the various kinds of carbonaceous materials with diverse morphology, 2D mesoporous carbon nanosheets (MCNs) with thin thickness, porous structure and unusual layered structure, abundant and accessible active site, open pores, as well as unique electronic properties, making them potential candidates for energy storage in supercapacitor [9–12]. Therefore, it is very important to construct MCNs reasonably, and some effective methods have been developed. The hard template method is the most effect approach for preparation of MCNs due to can be controlled by adjusting the size or shape of the template [13–15]. Many hard templates with layered structure have been used to prepare carbon sheets, such as porous silica, layered metal oxide, NaCl, $Mg(OH)_2$, MoS_2 nanosheets, and so on [16–18]. However, these templates must be synthesized before use, and they will be etched by a large amount of corrosive acids after carbonization, resulting in complex production processes and serious environmental pollution. In addition, the solvent including *N*, *N*-dimethylformamide, acetone, ethanol, tetrahydrofuran, or water, *etc.* are pre-requisite for assembling carbon precursors on hard templates. Unfortunately, the organic solvents using is harmful to the environment and the polymerization time is relatively long, making operations uncontrollable. The resin generally need polymerization, and formaldehyde is also the

* Corresponding authors.
E-mail addresses: chen_ab@163.com (A. Chen), housenlin2006@126.com (S. Hou).

https://doi.org/10.1016/j.cjche.2022.04.020
1004-9541/

needed raw in the polymerization reaction. However, formaldehyde is harmful to the environment and human health, which limits the development of resin-based materials for the production of MCNs [19,20]. Therefore, choosing an inexpensive template and simplifying the preparation process are the inevitable choices for the hard template to prepare MCNs.

Herein, we developed a self-deposition process that directly uses 3-aminophenol (3-AF) monomers as carbon precursors and cheap $Mg(OH)_2$ as hard templates to prepare N-doped mesoporous carbon nanosheets (N-MCNs) by solid grinding. Unlike the previous template methods, we use monomer as carbon precursor with avoiding the utilization of solvents and toxic formaldehyde to simplify the preparation process. Under the action of the catalytic $Mg(OH)_2$ nanosheet, the 3-AF monomer can be directly converted into the carbon skeleton on the template surface during the pyrolysis process. Moreover, the solid grinding process is convenient for large-scale production as a solvent-free method. The obtained N-MCNs completely copy the template's morphologies, possesses uniform mesoporous, high surface area and N-doping, which will benefit for high diffusion of ions and improve the electrochemical performance as electrode materials in supercapacitor.

2. Experimental

2.1. Materials

Magnesium chloride hexahydrate ($MgCl_2{\cdot}6H_2O$), sodium carbonate (Na_2CO_3), and hydrochloric acid (HCl, 36% (mass)) were purchased from Tianjin Yongda Chemical Corp., China. 3-Aminophenol was purchased from Aladdin Corp., China.

2.2. Preparation of $Mg(OH)_2$ sheets

Na_2CO_3 solution was dropwise added to $MgCl_2$ solution under continuous stirring (Na_2CO_3 and $MgCl_2$ with 1:1 molar ratio). After stirring at room temperature for 4 h, the precipitate $MgCO_3$ was collected by centrifugation, followed by washing and drying of the sample. MgO rods were then obtained by calcining $MgCO_3$ under air atmosphere at 500 °C for 2 h. 0.2 g the as-prepared MgO rods were homogeneously dispersed in 120 ml deionized water and stirred for 3 h, the precipitate $Mg(OH)_2$ sheets were collected by centrifugation, followed by washing and drying of the sample.

2.3. Preparation of N-MCNs

N-MCNs were prepared *via* the template method using $Mg(OH)_2$ as the template and 3-aminophenol (3-AF) as carbon and nitrogen precursors. Typically, for preparation of N-MCNs-1, 0.5 g $Mg(OH)_2$ and 0.5 g 3-AF were mixed by grinding for 20 min in an agate mortar. Subsequently, the 3-AF/$Mg(OH)_2$ composite was carbonized by heat treatment at 800 °C with rate of 5 °C·min^{-1}. The N-MCNs was obtained after etching the templates by 2 mol·L^{-1} HCl solution. The mass ratios of $Mg(OH)_2$/3-AF were 1:0.5, 1:1, 1:2, and the obtained samples were named N-MCNs-0.5, N-MCNs-1, and N-MCNs-2, respectively.

2.4. Characterization

Scanning electron microscopy (SEM) analysis was conducted using an S-4800-I (Hitachi, Japan) scanning electron microscope. The morphology and microstructure of samples were investigated by transmission electron microscopy (TEM, JEM-2100, JEOL, Japan). Nitrogen adsorption–desorption isotherms were carried out on a TriStar 3020 instrument (Micromeritics, USA) at −196 °C. The Brunauer–Emmett–Teller method was used to calculate the specific surface area, while the Barrett–Joyner–Halenda method was applied to analyze the pore size distribution using the desorption branch of isotherm. The total pore volume was obtained from the amount of N_2 adsorbed at the relative pressure (P/P_0 = 0.97). X-ray photoelectron spectroscopy (XPS) was conducted on a ESCALab 250Xi system (Thermo Fisher Scientific, USA) using an Al-K_α radiation under a vacuum of 3×10^{-8} Pa.

2.5. Electrochemical measurements

The working electrode was prepared by coating the viscous slurry (samples, carbon black and polytetrafluoroethylene with the mass ratio of 8:1:1 in ethanol) onto a Ni foam current collector. The mass of active material loaded on each working electrode was 4–5 mg after drying at 100 °C for 12 h. Electrochemical measurements were carried out in both three-electrode and two-electrode systems using an electrochemical workstation (CHI 760E, Chenhua Instruments, Shanghai, China) with 6 mol·L^{-1} KOH solution as the electrolyte. For the three-electrode system, Pt wire and Hg/HgO were used as the counter and reference electrodes. For the fabrication of supercapacitor devices, two slices of electrodes were immersed in 1 mol·L^{-1} Na_2SO_4 and were separated by a filtration paper, then tested by the current collector.

Electrochemical performances were evaluated by cyclic voltammetry (CV), galvanostatic charge–discharge (GCD), and electrical impedance spectroscopy (EIS) analysis. For the two-electrode system, the specific capacitances (C, F·g^{-1}), energy density (E, W·h·kg^{-1}), and power density (P, W·kg^{-1}) were calculated by the following equations: $C = I\Delta t/\Delta Vm$, $E = 0.5C\ (\Delta V)^2/3.6$ and $P = E/\Delta t$, where I (A), Δt (s), ΔV (V), and m (g) are GCD current, discharge time, voltage window, and mass of the active material, respectively. In the three-electrode system, the specific gravimetric capacitance according to the GCD measurements: $C = I\Delta t/\Delta Vm$.

3. Results and Discussion

3.1. Characterization of N-MCNs samples

Fig. 1(a) shows the fabrication processes of N-MCNs by self-deposition strategy using 3-AF monomer as carbon precursor and $Mg(OH)_2$ as template. The carbon precursor of 3-AF monomer was mixed with $Mg(OH)_2$ nanosheets by simple solid–solid grinding. The 3-AF can be adsorbed by $Mg(OH)_2$ nanosheets due to the interaction between hydroxyl group in $Mg(OH)_2$ and amino in 3-AF. During pyrolysis (Fig. 1(b)), 3-AF will be decomposed into small molecular carbon species while $Mg(OH)_2$ is gradually decomposed with increasing temperature and is transformed into MgO (Fig. 1(c)) [16]. Owing to the catalysis of Mg species on carbon deposition, the small molecular carbon species will be deposited on the MgO nanosheets, forming composites of MgO and carbon (Fig. 1(d)) [21,22]. In addition, due to the inhomogeneous deposition of carbon and shrinkage of $Mg(OH)_2$, the carbon layer shows rich mesoporous structure.

Fig. 1(e) illustrated the SEM images of N-MCNs-1 obtained by mass ration of $Mg(OH)_2$ to 3-AF. The SEM image of $Mg(OH)_2$ can be seen from Fig. S1 (in Supplementary Material), indicating its irregular nanosheets and the realization of carbon deposition on $Mg(OH)_2$ nanosheets. The crude surface of N-MCNs-1 indicted the uneven deposition of carbon precursors. From the low-magnification TEM image (Fig. 1(f)), the N-MCNs-1 shows inter-

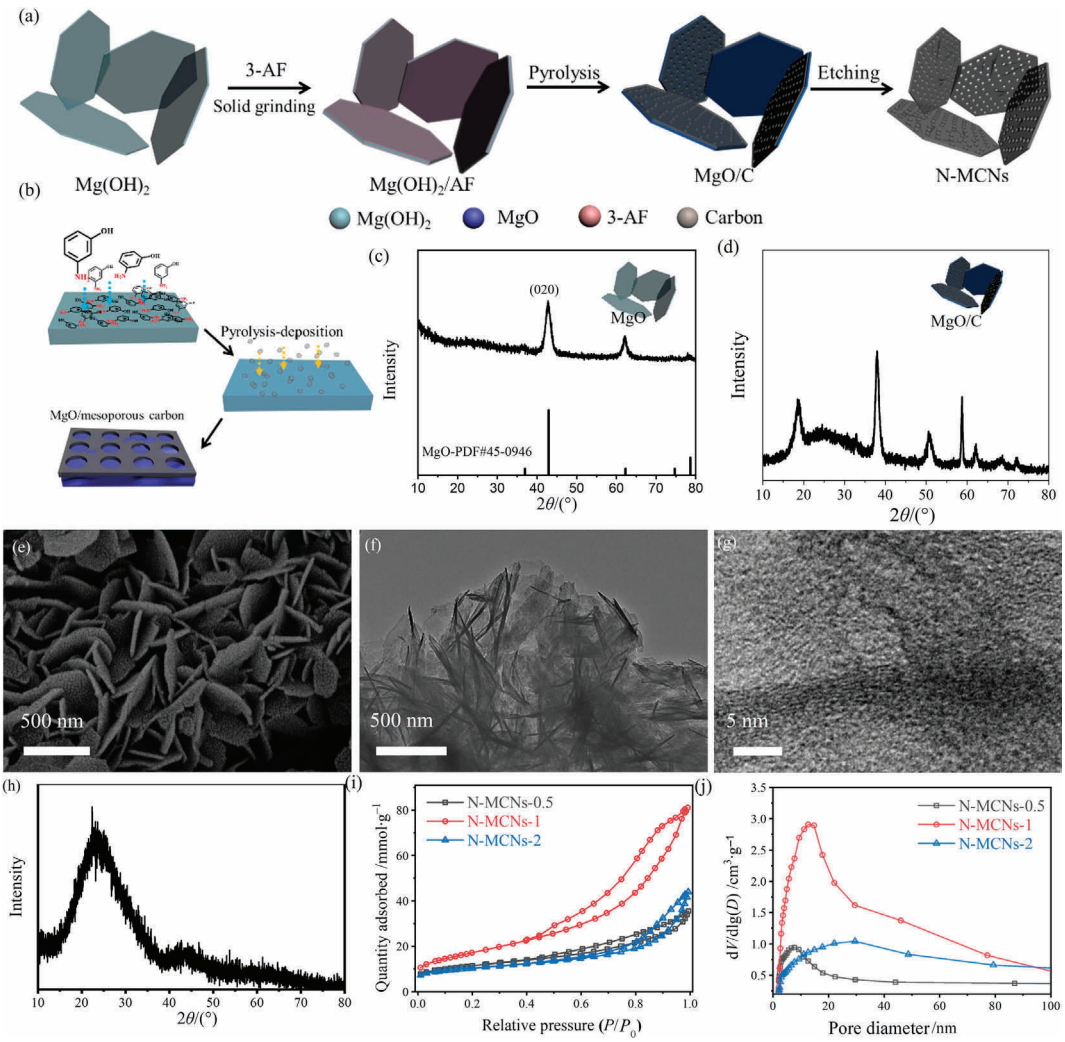

Fig. 1. Illustration of the synthesis routes for N-MCNs (a,b); XRD patterns of MgO (c) and MgO/C (d); SEM image (e), TEM images (f,g), and XRD pattern (h) of N-MCNs-1; and N_2 adsorption–desorption isotherms (i) and pore distribution (j) of the N-MCNs.

secting sheet with rich mesoporous. Furthermore, N-MCNs-1 also shows a certain graphitization structure seen from Fig. 1(g) due to the catalysis of MgO at high temperature [14]. To confirm the structure of N-MCNs-1, XRD patterns are depicted in Fig. 1(h). Two broad diffraction peaks can be observed around 26° and 43°, which can be assigned to the planes of graphitization structure, consisting with the TEM.

Moreover, the mass ration of $Mg(OH)_2$ to 3-AF also plays an important role for the mesoporous structure. The textural properties of N-MCNs were analyzed by nitrogen isothermal adsorption–desorption measurements. The isotherm of N-MCNs (Fig. 1(i)) shows a type of IV adsorption–desorption isotherm with obvious H3 hysteresis loops in the range of *ca.* 0.4–0.9 P/P_0, suggesting the presence of a large number of mesoporous [23,24]. Furthermore, the corresponding pore size distribution curve of N-MCNs confirms its mesoporous with pore size of ~4.6 nm as shown in Fig. 1(j). Moreover, another pore size also can be found at 10.1–15.6 nm, which may be attributed to the stacking of sheets. The detail properties of N-MCNs sample was presented in Table 1. It is obvious that these N-MCNs samples possess a large percentage

Table 1
Detail properties of N-MCNs.

Sample	S_{BET}/m²·g⁻¹	S_{micro}①/m²·g⁻¹	V_t②/cm³·g⁻¹	V_{micro}③/cm³·g⁻¹	Pore size④/nm
N-MCNs-0.5	872	411	1.2	0.13	4.6
N-MCNs-1	1387	612	2.8	0.13	4.6/15.9
N-MCNs-2	774	377	1.5	0.13	4.6/15.6

① Micropore surface area determined by the *t*-plot.
② Total pore volume at P/P_0-0.99.
③ Micropore volume.
④ BJH method was applied to analyze the pore size distribution using the desorption branch of the isotherm.

of mesoporous structures. Mesoporous carbon architectures are suitable candidates for exploring supercapacitor performance with various kinds of electrolytes. The N-MCNs-1 shows the highest specific surface area and pore volume, indicating proper mass ratio of $Mg(OH)_2$ to 3-AF is crucial to its porous structure. The N-MCNs-0.5 shows a smaller specific surface area, which might be due to insufficient carbon precursor filling the hard template. At the same time, the surface area of N-MCNs-2 also decreases slightly, indicating that too many monomers lead to low efficiency. Using this self-deposition method, carbon nano rod (N-CR) also can be prepared using MgO rod as hard template. As show in Fig. S2(a), the N-CR had a rod-like structure. In addition, the N_2 adsorption isotherm (Fig. S2(b)) with a typical H3 hysteresis loop and pore distribution (Fig. S2(c)) confirm its mesoporous structure.

XPS was used to further study the surface composition of N-MCNs-1, and the corresponding test results are shown in Fig. 2. Three peaks at 284.9, 532.3, and 400.9 eV were corresponded to C 1s, N 1s, and O 1s in N-MCNs-1 (Fig. 2(a)), respectively. As estimated by the XPS results, the atom percent of nitrogen is 1.5 for N-MCNs-1. In C 1s spectra, four sub-peaks of C═O, C—O, C—N/C—C, and graphitic C at 289.9, 286.1, 285.5, and 284.6 eV can be deconvoluted (Fig. 2(b)). High-resolution O 1s spectra for the N-MCNs-1 reveals the assignments of three types of O defects (Fig. 2(c)), corresponding to C═O, C—O and hydroxyl oxygen at 532.9, 531.1 and 534.7 eV, respectively. As shown in Fig. 2(d), three binding energies of 398.2, 400.2 and 404.0 eV can be attributed to pyridinic-N, pyrrolic-N, and quaternary-N in N-MCNs-1, respectively [25,26].

3.2. Electrochemical performance of N-MCNs samples

The features of regular flake morphology, porous structure, high specific surface area and N-containing functional groups can shorten the distance of charge transfer and increase the electronic charge density of carbon and favor proton adsorption in the acidic electrolyte, which make it have good performance in supercapacitors [27–32]. The supercapacitor performance N-MCNs based electrode was tested in a three-electrode system. As illustrated in Fig. 3(a), calculated from the CV area, the N-MCNs-1 shows the capacitance. At current density of 1 $A{\cdot}g^{-1}$, the GCD tests of N-MCNs were carried out as shown in Fig. 3(b) and calculated by discharge branches at 1 $A{\cdot}g^{-1}$ (Fig. 3(b)), the specific capacitance of N-MCNs-1 electrode is 240 $F{\cdot}g^{-1}$, which is larger than that of N-MCNs-0.5 (162 $F{\cdot}g^{-1}$) and N-MCNs-2 (175 $F{\cdot}g^{-1}$). The rectangular shape of CV curves and isosceles triangle of GCD curves indicated the co-existence of electric double layer capacitance (EDLC) and pseudo capacitance behaviors. There is no obvious redox peak in the CV and GCD plots due to the co-existence of three types of nitrogen species leads to multiple faradaic peaks [33–37]. Fig. 3(c) shows their good rate capability at the current density from 1 to 50 $A{\cdot}g^{-1}$. Among them, the N-MCNs-1 exhibited highest rate capability (75.4%) and capacitance, which may attribute to its largest specific surface area and the matching pore structure. At the open-circuit voltage, further EIS measurements were conducted (Fig. 3(d)). At the characteristic feature of pure capacitive behavior can be seen from the low frequency region with inclined line [20,38–40]. In addition, the fitted result distinctly showed that the internal resistance values were 0.77, 0.59 and 0.90 Ω for N-MCNs-0.5, N-MCNs-1, and N-MCNs-2, respectively. The results indicated the advantage of rich mesoporous channel for ion storage and transportation.

At the scanning rate ranges of 5–200 $mV{\cdot}s^{-1}$ the CV curves with nearly rectangular shape for the N-MCNs-1 electrode was obtained in the potential window of −1.0 to 0 V as shown in Fig. S3(a), indicating its good capacitance performance. The GCD curves indicated a good capacitance performance of N-MCNs-1 electrode at a current density of 1–20 $A{\cdot}g^{-1}$ as illustrated in Fig. S3(b). As seen, a small voltage drop (IR drop) of 0.08 V at 20 $A{\cdot}g^{-1}$ proved the fast

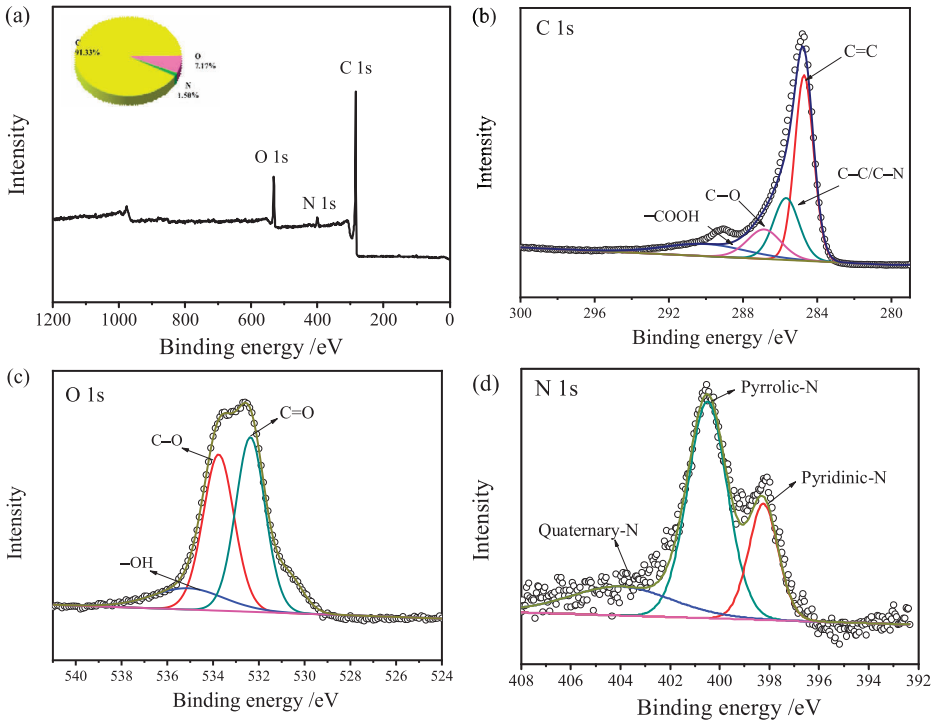

Fig. 2. XPS pattern of N-MCNs-1 (a); C 1s (b), O 1s (c) and N 1s (d) spectra of N-MCNs-1.

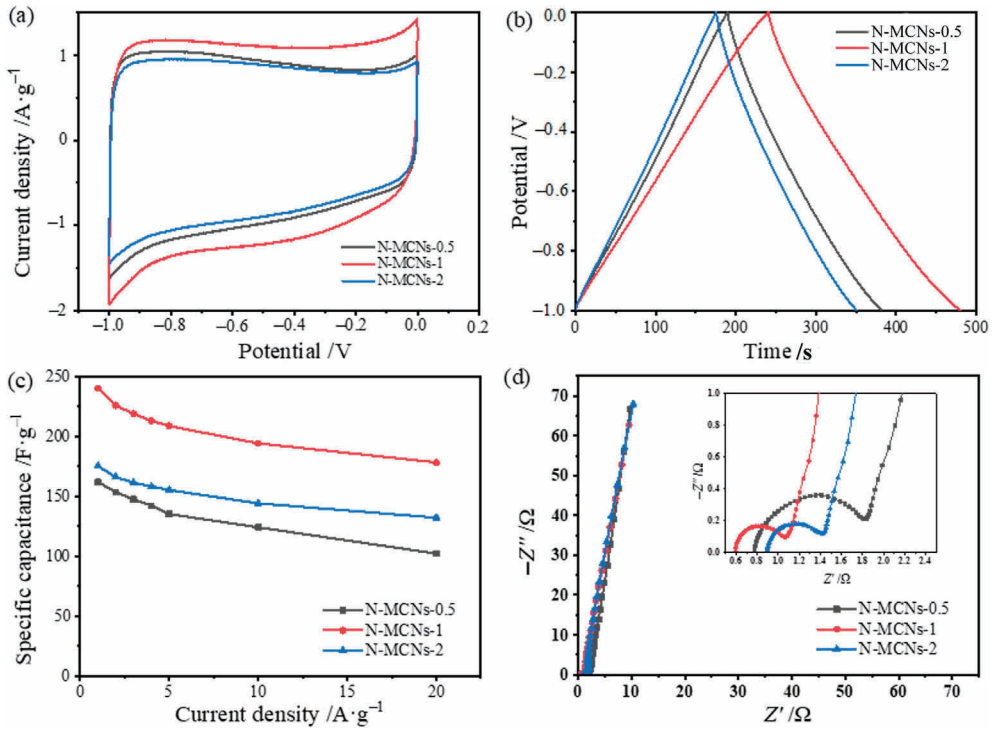

Fig. 3. Electrochemical evaluation of the N-MCNs-1 with different rate of monomer/template: (a) CV curves; (b) GCD curves; (c) specific capacitances; (d) Nyquist plots.

ion transportation. Some shape deformations can be observed in both GCD and CV curves due to the presence of Faradaic effects derived from N-doping features. As plotted in Fig. S3(c), N-MCNs-1 shows a high capacitance retention rate of 98.3% after 10,000 times of continuous cycling at 5 $A \cdot g^{-1}$. The GCD curves of the last 10 cycles were almost similar with the first 10 cycles (Fig. S3(c) inset), which are linear and symmetrical, and show excellent capacitance performance and long-term electrochemical stability.

Two-electrode cell was also fabricated to investigate the electrochemical performance of supercapacitor in practical applications based on N-MCNs-1 electrode. The Na_2SO_4 electrolyte can effectively prevent electrode materials floating for a long period from corrosion and enable a higher working voltage for carbon-based electrode by reducing capacity attenuation. Moreover, there is a positive correlation between working voltage and energy density. Therefore, the symmetric supercapacitor cell based on N-MCNs-1 material is performed in 1 $mol \cdot L^{-1}$ Na_2SO_4 electrolyte. CV curves are performed in different voltage ranges to determine the optimal and stable operating voltage range. Fig. 4(a) shows the CV curves of as-fabricated symmetric supercapacitors at a scan rate of 50 $mV \cdot s^{-1}$ in various voltage ranges. At ranges from 0.8 V to 1.8 V, GCD curves of symmetric supercapacitor (Fig. 4(b)) also confirm that the ideal electrochemical reversibility. Thus, these above data suggest that the optimal operating voltage range is 1.6 V.

Fig. 4(c) shows the typical capacitance values of symmetric supercapacitors at different scanning rates from 5 to 200 $mV \cdot s^{-1}$. The CV curves with not changing significantly at a high scan rate of 200 $mV \cdot s^{-1}$, indicating the remarkable rate performance probably owing to the rich mesoporous structure. For the assembled symmetric supercapacitor, the effective accessibility of electrolyte ions at high charge/discharge rates can be realized. Furthermore, the galvanostatic charge/discharge profiles (Fig. 4(d)) of the N-MCNs-1 also show low IR drop (0.1 V), indicating excellent electrochemical reversibility and low internal series resistance. In the two-electrode cell, the specific capacitance of N-MCNs-1 182 $F \cdot g^{-1}$ at a current density of 1 $A \cdot g^{-1}$. Moreover, N-MCNs-1 possesses relative high capacitance retention of 35.7% (Fig. 4(e)) when current density increases from 1 to 20 $A \cdot g^{-1}$. Fig. 4(f) shows the Ragone plot of the two-electrode cell. The energy density is 18.2 $W \cdot h \cdot kg^{-1}$ at a power density of 400 $W \cdot kg^{-1}$ and the energy density of N-MCNs-1 is much higher than those of previously reported carbonaceous aqueous symmetric supercapacitor, such as N-doped carbon nanofibers *etc.*, showing the potential as a supercapacitor material [6,38,39,41–47].

4. Conclusions

In summary, the N-MCNs have been fabricated *via* self-deposition method using 3-AF monomer as carbon/nitrogen precursor, and $Mg(OH)_2$ as the hard template. This method can directly realize carbon formation from 3-AF monomer, avoiding the polymerization process of resin and the solvent in traditional methods. The prepared N-MCNs can completely replicate the morphologies of the $Mg(OH)_2$ template and shows high surface area, rich mesopores, pore volume and N-doping. These characteristics make N-MCNs great promising in supercapacitor with high capacitance, long cycle life and high energy density. This template method can be used to realize the self-deposition of monomer into carbon, which provides a new idea for the preparation of high-performance carbon-based materials with high efficiency, low cost, operability and easy implementation. It is also hoped that this N-MCNs will have a wide application prospect in adsorption separation or catalyst carrier, *etc.*

Declaration of Competing Interest

The authors declare that they have no known competing financial interests or personal relationships that could have appeared to influence the work reported in this paper.

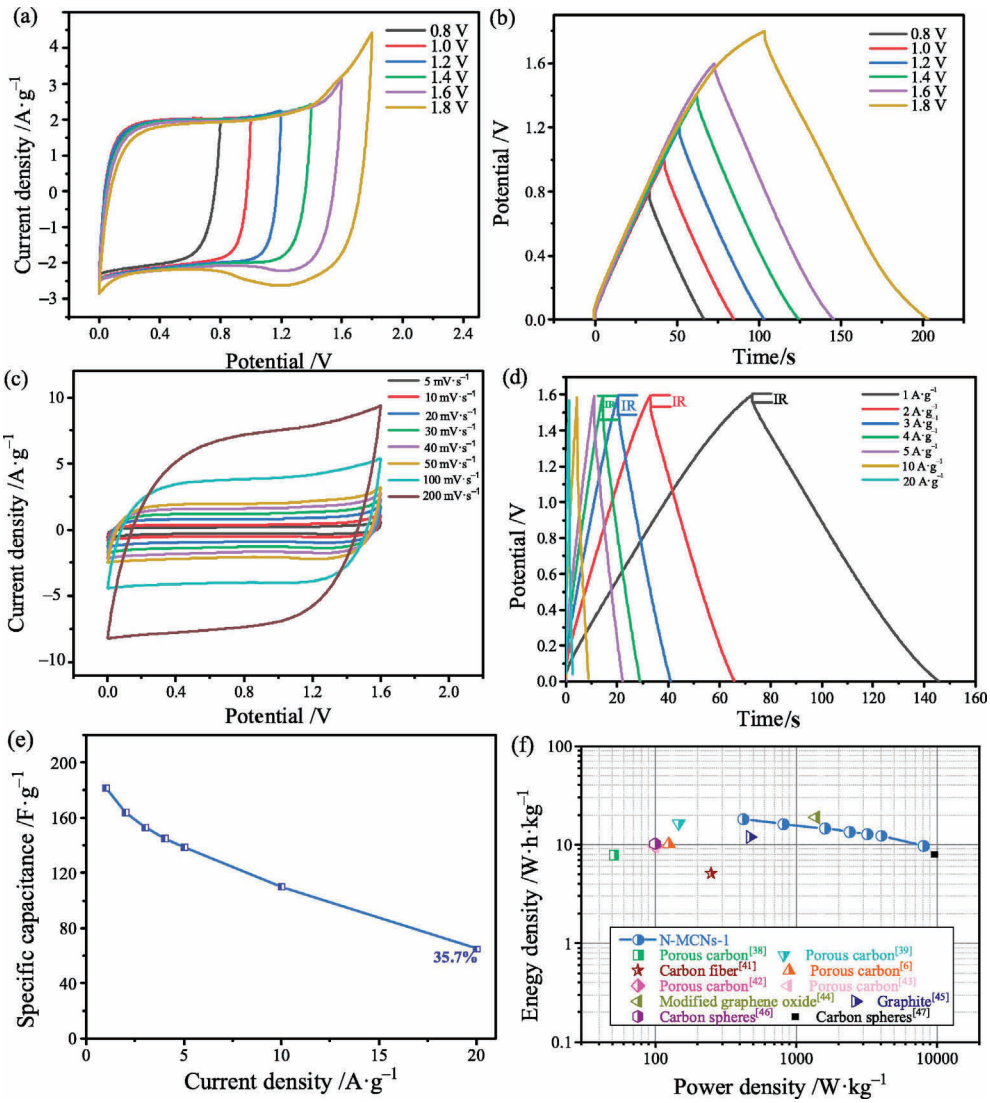

Fig. 4. CV curves at 50 mV·s^{-1} (a) and GCD curves at 1 A·g^{-1} (b) in different voltage windows for the N-MCNs-1, CV curves at different scan rates (c), GCD curves at different current densities (d) of N-MCNs-1, the specific capacitance of N-MCNs-1 at different current density (e) in two-electrode system and Ragone plots comparison with the reported carbon spheres with different structures of N-MCNs-1 (f).

Acknowledgements

We thank the Natural Science Foundation of Hebei (B02020208088), S&T Program of Hebei (20544401D, 20314401D, 206Z4406G, 21314402D, B2021208074, 21344601D), Tianjin Science and Technology Project (19YFSLQY00070).

Supplementary Material

Supplementary data to this article can be found online at https://doi.org/10.1016/j.cjche.2022.04.020.

References

[1] Y.J. Zhang, H.L. Chen, S.J. Wang, X. Zhao, F.G. Kong, Regulatory pore structure of biomass-based carbon for supercapacitor applications, *Micropor. Mesopor. Mater.* 297 (2020) 110032.
[2] S. Lv, L.Y. Ma, X.Y. Shen, H. Tong, One-step copper-catalyzed synthesis of porous carbon nanotubes for high-performance supercapacitors, *Micropor. Mesopor. Mater.* 310 (2021) 110670.
[3] W.M. Chen, M. Luo, K. Yang, X.Y. Zhou, Microwave-assisted KOH activation from lignin into hierarchically porous carbon with super high specific surface area by utilizing the dual roles of inorganic salts: Microwave absorber and porogen, *Micropor. Mesopor. Mater.* 300 (2020) 110178.
[4] H. Li, Y.H. Zhao, S.Q. Liu, P.C. Li, D. Yuan, C.B. He, Hierarchical porous carbon monolith derived from lignin for high areal capacitance supercapacitors, *Micropor. Mesopor. Mater.* 297 (2020) 109960.
[5] Q.S. Wang, Y.F. Zhang, H.M. Jiang, X.J. Li, Y. Cheng, C.G. Meng, Designed mesoporous hollow sphere architecture metal (Mn Co, Ni) silicate: A potential electrode material for flexible all solid-state asymmetric supercapacitor, *Chem. Eng. J.* 362 (2019) 818–829.
[6] Y.H. Wang, R.N. Liu, Y.D. Tian, Z. Sun, Z.H. Huang, X.L. Wu, B. Li, Heteroatoms-doped hierarchical porous carbon derived from chitin for flexible all-solid-state symmetric supercapacitors, *Chem. Eng. J.* 384 (2020) 123263.
[7] W. Yan, Z.H. Meng, M.Y. Zou, H. Miao, F.X. Ma, R. Yu, W. Qiu, X.Y. Liu, N.B. Lin, Neutralization reaction in synthesis of carbon materials for supercapacitors, *Chem. Eng. J.* 381 (2020) 122547.
[8] H.J. Li, Q.S. Miao, Y.L. Chen, M.Y. Yin, H. Qi, M.C. Yang, Q.L. Deng, S. Wang, Modified carbon spheres as universal materials for adsorption of cationic harmful substances (paraquat and dyes) in water, *Micropor. Mesopor. Mater.* 297 (2020) 110040.
[9] Y.F. He, X.D. Zhuang, C.J. Lei, L.C. Lei, Y. Hou, Y.Y. Mai, X.L. Feng, Porous carbon nanosheets: Synthetic strategies and electrochemical energy related applications, *Nano Today* 24 (2019) 103–119.
[10] L.L. Zou, C.C. Hou, Q.J. Wang, Y.S. Wei, Z. Liu, J.S. Qin, H. Pang, Q. Xu, A honeycomb-like bulk superstructure of carbon nanosheets for electrocatalysis and energy storage, *Angew. Chem. Int. Ed.* 59 (44) (2020) 19627–19632.
[11] C.C. Lei, C.C. Ji, H.Y. Mi, C.C. Yang, Q. Zhang, S.X. He, Z.Y. Bai, J.S. Qiu, Engineering kinetics-favorable carbon sheets with an intrinsic network for a

superior supercapacitor containing a dual cross-linked hydrogel electrolyte, *ACS Appl. Mater. Interfaces* 12 (47) (2020) 53164–53173.
[12] M. Wang, J. Yang, S.Y. Liu, M.Z. Li, C. Hu, J.S. Qiu, Nitrogen-doped hierarchically porous carbon nanosheets derived from polymer/graphene oxide hydrogels for high-performance supercapacitors, *J. Colloid Interface Sci.* 560 (2020) 69–76.
[13] H. Liu, D.D. Zhai, M. Wang, J.S. Liu, X.Y. Chen, Z.J. Zhang, Urea-modified phenol-formaldehyde resins for the template-assisted synthesis of nitrogen-doped carbon nanosheets as electrode material for supercapacitors, *ChemElectroChem* 6 (3) (2019) 885–891.
[14] X.J. He, N. Zhang, X.L. Shao, M.B. Wu, M.X. Yu, J.S. Qiu, A layered-template-nanospace-confinement strategy for production of corrugated graphene nanosheets from petroleum pitch for supercapacitors, *Chem. Eng. J.* 297 (2016) 121–127.
[15] W.D. Geng, F.W. Ma, G. Wu, S.J. Song, J.F. Wan, D. Ma, MgO-templated hierarchical porous carbon sheets derived from coal tar pitch for supercapacitors, *Electrochim. Acta* 191 (2016) 854–863.
[16] Z.M. Zheng, X. Zhang, F. Pei, Y. Dai, X.L. Fang, T.H. Wang, N.F. Zheng, Hierarchical porous carbon microrods composed of vertically aligned graphene-like nanosheets for Li-ion batteries, *J. Mater. Chem. A* 3 (39) (2015) 19800–19806.
[17] S. Zhu, J.J. Li, L.Y. Ma, L.C. Guo, Q.Y. Li, C.N. He, E.Z. Liu, F. He, C.S. Shi, N.Q. Zhao, Three-dimensional network of N-doped carbon ultrathin nanosheets with closely packed mesopores: Controllable synthesis and application in electrochemical energy storage, *ACS Appl. Mater. Interfaces* 8 (18) (2016) 11720–11728.
[18] T.Y. Wu, X.J. Wu, L.H. Li, M.M. Hao, G. Wu, T. Zhang, S. Chen, Anisotropic boron–carbon hetero-nanosheets for ultrahigh energy density supercapacitors, *Angew. Chem. Int. Ed.* 59 (52) (2020) 23800–23809.
[19] L. Yao, Q. Wu, P.X. Zhang, J.M. Zhang, D.R. Wang, Y.L. Li, X.Z. Ren, H.W. Mi, L.B. Deng, Z.J. Zheng, Scalable 2D hierarchical porous carbon nanosheets for flexible supercapacitors with ultrahigh energy density, *Adv. Mater.* 30 (11) (2018) 1706054.
[20] C. Chen, M.K. Zhao, Y.Y. Cai, G.Z. Zhao, Y. Xie, L. Zhang, G. Zhu, L.K. Pan, Scalable synthesis of strutted nitrogen doped hierarchical porous carbon nanosheets for supercapacitors with both high gravimetric and volumetric performances, *Carbon* 179 (2021) 458–468.
[21] G.C. Li, K. Mao, M. Liu, M.L. Yan, J. Zhao, Y. Zeng, L.J. Yang, Q. Wu, X.Z. Wang, Z. Hu, Achieving ultrahigh volumetric energy storage by compressing nitrogen and sulfur dual-doped carbon nanocages *via* capillarity, *Adv. Mater.* 32 (52) (2020) 2004632.
[22] C. Tang, H.F. Wang, X. Chen, B.Q. Li, T.Z. Hou, B.S. Zhang, Q. Zhang, M.M. Titirici, F. Wei, Topological defects in metal-free nanocarbon for oxygen electrocatalysis, *Adv. Mater.* 28 (32) (2016) 6845–6851.
[23] H. Zhang, F. Zhang, Y.Q. Wei, Q.C. Miao, A.Y. Li, Y.S. Zhao, Y. Yuan, N.F. Jin, G.H. Li, Controllable design and preparation of hollow carbon-based nanotubes for asymmetric supercapacitors and capacitive deionization, *ACS Appl. Mater. Interfaces* 13 (18) (2021) 21217–21230.
[24] N.T. Nguyen, P.A. Le, V.B.T. Phung, Biomass-derived carbon hooks on Ni foam with free binder for high performance supercapacitor electrode, *Chem. Eng. Sci.* 229 (2021) 116053.
[25] L. Yu, C.T. Hsieh, D.J. Keffer, H. Chen, G.A. Goenaga, S. Dai, T.A. Zawodzinski, D. P. Harper, Hierarchical lignin-based carbon matrix and carbon dot composite electrodes for high-performance supercapacitors, *ACS Omega* 6 (11) (2021) 7851–7861.
[26] Z. Yan, Z. Gao, Z. Zhang, C. Dai, W. Wei, P.K. Shen, Graphene nanosphere as advanced electrode material to promote high performance symmetrical supercapacitor, *Small* 17 (18) (2021) e2007915.
[27] M.X. Wang, J. Zhang, X.B. Yi, X.F. Zhao, B.X. Liu, X.C. Liu, Nitrogen-doped hierarchical porous carbon derived from ZIF-8 supported on carbon aerogels with advanced performance for supercapacitor, *Appl. Surf. Sci.* 507 (2020) 145166.
[28] Z. Shang, X.Y. An, H. Zhang, M.X. Shen, F. Baker, Y.X. Liu, L.Q. Liu, J. Yang, H.B. Cao, Q.L. Xu, H.B. Liu, Y.H. Ni, Houttuynia-derived nitrogen-doped hierarchically porous carbon for high-performance supercapacitor, *Carbon* 161 (2020) 62–70.
[29] X.Y. Qian, L. Miao, J.X. Jiang, G.C. Ping, W. Xiong, Y.K. Lv, Y.F. Liu, L.H. Gan, D.Z. Zhu, M.X. Liu, Hydrangea-like N/O codoped porous carbons for high-energy supercapacitors, *Chem. Eng. J.* 388 (2020) 124208.
[30] X.T. Meng, S. Jia, L.L. Mo, J. Wei, F.J. Wang, Z.Q. Shao, O/N-co-doped hierarchically porous carbon from carboxymethyl cellulose ammonium for high-performance supercapacitors, *J. Mater. Sci.* 55 (17) (2020) 7417–7431.
[31] S.J. Meng, Z.L. Mo, Z.L. Li, R.B. Guo, N.J. Liu, Oxygen-rich porous carbons derived from alfalfa flowers for high performance supercapacitors, *Mater. Chem. Phys.* 246 (2020) 122830.
[32] W.W. Fu, K. Zhang, M.S. Chen, M. Zhang, Z.R. Shen, One-pot synthesis of N-doped hierarchical porous carbon for high-performance aqueous capacitors in a wide pH range, *J. Power Sources* 491 (2021) 229587.
[33] Y. Li, Q.L. Wei, R. Wang, J.K. Zhao, Z.L. Quan, T.R. Zhan, D.X. Li, J. Xu, H.N. Teng, W.G. Hou, 3D hierarchical porous nitrogen-doped carbon/Ni@NiO nanocomposites self-templated by cross-linked polyacrylamide gel for high performance supercapacitor electrode, *J. Colloid Interface Sci.* 570 (2020) 286–299.
[34] J.G. Kim, H.C. Kim, N.D. Kim, M.S. Khil, N-doped hierarchical porous hollow carbon nanofibers based on PAN/PVP@SAN structure for high performance supercapacitor, *Compos. B Eng.* 186 (2020) 107825.
[35] H.Y. Jia, S. Qiu, W.Y. Li, D.D. Liu, X. Xie, Heteroatom-doped porous carbon derived from low-cost precursors of egg juice and commercial polymeric adsorbent as superior material for high performance supercapacitor, *J. Electroanal. Chem.* 863 (2020) 114057.
[36] H.Y. Jia, S. Qiu, F. Hu, L.C. Wang, J.S. Shi, X. Xie, Adsorption-doping for preparing N-doped porous carbon for promising electrochemical capacitors-using peptone and polymer porous resin as precursors, *J. Energy Storage* 28 (2020) 101297.
[37] J.H. Jeong, Y.A. Kim, B.H. Kim, Electrospun polyacrylonitrile/cyclodextrin-derived hierarchical porous carbon nanofiber/MnO_2 composites for supercapacitor applications, *Carbon* 164 (2020) 296–304.
[38] D. Dong, Y.S. Zhang, Y. Xiao, T. Wang, J.W. Wang, W. Gao, Mechanochemistry coupled with $MgCO_3$ one-step activation to prepare coal-based hierarchical porous carbon for supercapacitors, *J. Power Sources* 503 (2021) 230049.
[39] M.L. Cao, Q.X. Wang, W.L. Cheng, S.Q. Huan, Y. Hu, Z.X. Niu, G.P. Han, H.T. Cheng, G. Wang, A novel strategy combining electrospraying and one-step carbonization for the preparation of ultralight honeycomb-like multilayered carbon from biomass-derived lignin, *Carbon* 179 (2021) 68–79.
[40] T.T. Zhu, J. Zhou, Z.H. Li, S.J. Li, W.J. Si, S.P. Zhuo, Hierarchical porous and N-doped carbon nanotubes derived from polyaniline for electrode materials in supercapacitors, *J. Mater. Chem. A* 2 (31) (2014) 12545.
[41] L. Chen, Z.Y. Wen, L.N. Chen, W.P. Wang, Q. Ai, G.M. Hou, Y.H. Li, J. Lou, L.J. Ci, Nitrogen and sulfur co-doped porous carbon fibers film for flexible symmetric all-solid-state supercapacitors, *Carbon* 158 (2020) 456–464.
[42] Y. Sun, J.J. Xue, S.Y. Dong, Y.D. Zhang, Y.F. An, B. Ding, T.F. Zhang, H. Dou, X.G. Zhang, Biomass-derived porous carbon electrodes for high-performance supercapacitors, *J. Mater. Sci.* 55 (12) (2020) 5166–5176.
[43] Y.L. Zhao, M.Z. Wei, Z.Z. Zhu, J. Zhang, L.Q. Xiao, L.X. Hou, Facile preparation of N-O codoped hierarchically porous carbon from alginate particles for high performance supercapacitor, *J. Colloid Interface Sci.* 563 (2020) 414–425.
[44] J.Q. Wang, Q. Li, C. Peng, N. Shu, L. Niu, Y.W. Zhu, To increase electrochemical performance of electrode material by attaching activated carbon particles on reduced graphene oxide sheets for supercapacitor, *J. Power Sources* 450 (2020) 227611.
[45] Y.N. Gong, D.L. Li, Q. Fu, Y.P. Zhang, C.X. Pan, Nitrogen self-doped porous carbon for high-performance supercapacitors, *ACS Appl. Energy Mater.* 3 (2) (2020) 1585–1592.
[46] H. Zhou, Y.M. Zhou, S.M. Wu, L. Li, Y.H. Li, M.X. Guo, Z.C. Qi, C.X. Feng, Synthesis of N/S co-doped porous carbon microspheres based on amino acid protic salt for supercapacitor, *J. Alloys Compd.* 829 (2020) 154549.
[47] J. Wen, X.P. Chen, M.L. Huang, W. Yang, J. Deng, Core–shell-structured MnO_2@carbon spheres and nitrogen-doped activated carbon for asymmetric supercapacitors with enhanced energy density, *J. Chem. Sci.* 132 (1) (2019) 1–11.